SINGULAR CURVES – A HIDDEN DYNAMICS REVEALING DNA STRUCTURE OF SHAPES

DRAFT AS OF November 3, 2012

MOODY T. CHU* AND ZHENYUE ZHANG†

Abstract. The importance of DNA to living organisms and its general structure of a double helix joined by base pairings whose sequences encode the genetic information are well known facts. Demonstrated in this article, via elementary calculus, is that there is a remarkably similar structure underneath all smooth surfaces. Such a structure exists even in higher dimensional spaces. Here we show that, analogous to the double helix structure with two (AT and CG) base parings in DNA, two strands of curves and eight base pairings would encode properties of an arbitrary surface. The idea is based on generalizing the common notion of gradient adaption from a scalar field to vector fields — singular vectors of the Jacobian of any given function form a natural moving frame pointing in directions along which the function varies most critically. Trajectories of these singular vectors, referred to as singular curves, unveil some interesting, perplexing, intriguing patterns per the given function. At points where two or more singular values coalesce, curious and complex behavior occurs, manifesting specific landmarks for the underlying function. This paper reports for the first time such an innate dynamical structure and, thus, raises the curiosity of whether the double strands with base pairings would be the universal structure encoding all 3-dimensional entities, life or lifeless. We anticipate that with our theory surfaces can be genome sequenced and classified accordingly.

Key words. singular curves, critical curves, gradient adaption, singular value decomposition, base pairings, DNA structure

AMS subject classifications. 37B35, 37N30, 65L07, 65D18, 53A05

1. Introduction.

Given a scalar function $\eta : \mathbb{R}^n \longrightarrow \mathbb{R}$, its gradient defined by

$$\nabla\eta(\mathbf{x}) := \left[\frac{\partial\eta}{\partial x_1}, \ldots, \frac{\partial\eta}{\partial x_n}\right]$$

points in the steepest ascent direction for the function value $\eta(\mathbf{x})$ with the maximum rate exactly equal to the Euclidean norm $\|\nabla\eta(\mathbf{x})\|$ of the gradient vector. The notion of gradient has a significant meaning in applications. Heat transfer by conduction, for example, is opposite to the temperature gradient which is perpendicular to the isothermal surfaces. Osmosis or passive transport across the cell membrane characterizes the movement of substances down a concentration gradient without requiring energy use. Image gradients representing directional change in the intensity or color, on the other hand, are used as the fundamental building blocks in image processing such as edge detection and computer vision.

A natural generalization of the gradient of a scalar function to a vector function $f : \mathbb{R}^n \longrightarrow \mathbb{R}^m$ is the Jacobian matrix defined by

$$f'(\mathbf{x}) := \begin{bmatrix} \frac{\partial f_1}{\partial x_1} & \cdots & \frac{\partial f_1}{\partial x_n} \\ \vdots & \ddots & \vdots \\ \frac{\partial f_m}{\partial x_1} & \cdots & \frac{\partial f_m}{\partial x_n} \end{bmatrix}.$$

The rate of change along any given unit vector $\mathbf{u}$ then can be measured via the norm of the directional derivative

$$\lim_{t\to 0}\left\|\frac{f(\mathbf{x}+t\mathbf{u})-f(\mathbf{x})}{t}\right\| = \|f'(\mathbf{x})\mathbf{u}\|. \tag{1.1}$$

*Department of Mathematics, North Carolina State University, Raleigh, NC 27695-8205. (chu@math.ncsu.edu)
This research was supported in part by the NSF grant DMS-1014666.
†Department of Mathematics, Zhejiang University, Hangzhou, Zhejiang 310027, China. (zyzhang@zju.edu.cn)
This research was supported in part by the NSFC project 11071218.

The question then arises on which direction points to the swiftest change and how much the maximum rate is attained. The answer lies in the notion of singular value decomposition (SVD) of the Jacobian matrix $f'(\mathbf{x})$.

Any given matrix $A \in \mathbb{R}^{m\times n}$ enjoys a factorization of the form

$$A = V\Sigma U^\top, \tag{1.2}$$

where $V \in \mathbb{R}^{m\times m}$ and $U \in \mathbb{R}^{n\times n}$ are orthogonal matrices, $\Sigma \in \mathbb{R}^{m\times n}$ is zero everywhere except for the nonnegative elements $\sigma_1 \geq \sigma_2 \geq \ldots \geq \sigma_\kappa > \sigma_{\kappa+1} = \ldots = 0$ along the leading diagonal with $\kappa = \operatorname{rank}(A)$. The scalars σ_i and the corresponding columns in U and V are called the singular values, the right, and the left singular vectors of A, respectively [4]. The notion of SVD has long been conceived in various disciplines [13] as it appears frequently in a remarkably wide range of important applications — data analysis [3], dimension reduction [10], signal processing [14], image compression, principal component analysis [16], to name but a few .

Among multiple ways to characterize the SVD of a matrix A, one is the variational formulation,

$$\max_{\|\mathbf{u}\|=1} \|A\mathbf{u}\|, \tag{1.3}$$

that sheds light on an important geometric property. One can show that the unit stationary points $\mathbf{u}_i \in \mathbb{R}^n$ for problem (1.3) and the associated objective values $\|A\mathbf{u}_i\|$ are exactly the right singular vectors and the singular values of A. By duality, there exists a unit vector $\mathbf{v}_i \in \mathbb{R}^m$ such that $\mathbf{v}_i^\top A\mathbf{u}_i = \sigma_i$. This $\mathbf{v}_i$ is the corresponding left singular vector of A. Taking the view that the linear map A transforms the unit sphere into an ellipsoid, then the right singular vectors $\mathbf{u}_i$'s point in the pivotal directions along which the semi-axis directions $\mathbf{v}_i$'s are attained and the singular values measure the extent of deformation. In this way, it is thus understood that the SVD information of the $f'(\mathbf{x})$ indicates the infinitesimal deformation property of the nonlinear map f at $\mathbf{x}$.

Certainly, there are other more sophisticated means to extract fingerprints of surfaces. We mention an interesting approach in [12] using Laplace-Beltrami spectra as an isometry-invariant shape descriptor. There is also the more classical approach employing conformal geometry [6] to perform surface parametrization, matching, tracking, identification, and so on [5]. We use elementary calculus only in this paper with the goal of pointing out a fascinating dynamics that is inherent to every smooth function.

At every point $\mathbf{x}$ in the domain space, we now have in hand a set of orthonormal vectors pointing in particular directions related to the variation of f. These orthonormal vectors form a natural frame point by point []. Tracking down the "motion" of these frames might help to reveal some innate peculiarities of the underlying function f. Thus, we are interested in the solution flows $\mathbf{x}_i(t) \in \mathbb{R}^n$ defined by

$$\dot{\mathbf{x}}_i := \pm\mathbf{u}_i(\mathbf{x}_i), \quad \mathbf{x}_i(0) = \widetilde{\mathbf{x}}, \tag{1.4}$$

or the corresponding $\mathbf{y}_i(t) \in \mathbb{R}^m$ defined by

$$\dot{\mathbf{y}}_i := \pm\sigma_i(\mathbf{x}_i)\mathbf{v}_i(\mathbf{x}_i), \quad \mathbf{y}_i(0) = f(\widetilde{\mathbf{x}}), \tag{1.5}$$

where $(\sigma_i, \mathbf{u}_i, \mathbf{v}_i)$ is the ith singular triplet of $f'(\mathbf{x}_i)$. The scaling in (1.5) is to ensure that $\mathbf{y}_i(t) = f(\mathbf{x}_i(t))$. The sign $\pm$ in defining the vector field is meant to select the direction so as to avoid discontinuity jump. Indeed, if we define $\mathbf{z}(t) := \mathbf{x}(-t)$ when $\dot{\mathbf{x}}(t) = \mathbf{u}(\mathbf{x}(t))$, then $\dot{\mathbf{z}}(t) = -\mathbf{u}(\mathbf{z}(t))$. We thus may assume, without loss of generality, that a direction of singular vectors has been predestined and that the time t can move either forward or backward. Even so, the right side of (1.4) (or (1.5)) may not be well defined at points when singular values coalesce, because then $f'(\mathbf{x})$ has multiple singular vectors corresponding to the same singular value, making $\dot{\mathbf{x}}_i$ (or $\dot{\mathbf{y}}_i$)

discontinuous. Such a discontinuity is different from the existence of an analytic factorization as a whole for a function analytic in $\mathbf{x}$ [1, 17]. The continuity of a fixed order singular vector, say, $\mathbf{u}_1(\mathbf{x})$, may not be maintained.

Because of the way they are constructed, we call the integral curves $\{\mathbf{x}_i(t)\}$ and $\{\mathbf{y}_i(t)\}$ the right and the left *singular curves* of the map f, respectively. This notion is different from that known as the principal curves [8, 7, 9]. What makes singular curves curious is that they represent some undercurrents of the functions not recognized before. These currents characterize the function and a function carries its own inherent flows. This work studies only the first singular curve $\mathbf{x}_1(t)$, yet preliminary investigations into its dynamics already reveal something remarkably amazing.

2. Examples of Singular Curves. Starting from any given $\widetilde{x} \in \mathbb{R}^n$, the first singular curve $\mathbf{x}_1(t)$ moves in the direction along which the function $f(\mathbf{x})$ changes most rapidly when measured in the Euclidean norm. It is the backbone axis in the moving frame. So as to facilitate conveying the wealth of intrigues of singular curves by graphs, we restrict our attention to the case $f : \mathbb{R}^2 \to \mathbb{R}^n$ which includes parametric surfaces in $\mathbb{R}^3$. We envision that the dynamics would be equally riveting in higher-dimensional spaces, but as a startup, we discuss only the basics with the hope of stimulating more interest into the general case later.

We choose to demonstrate the behavior of the eight functions listed in Table 2.1, each representing some peculiar features. Starting at uniform grid points over the domain $[-5, 5] \times [-5, 5]$ with mesh size .5, we integrate the system (1.4) up to $|t| = 30$ whenever possible in both directions. Local error tolerance for the numerical integrator ODE113 available in MATLAB is set at 10^{-12}, which should furnish reasonably high precision in tracking these curves. The corresponding singular curves $\mathbf{x}_1(t)$ are plotted in Figure 2.1. Since the tangent vector on the right side of (1.4) is always of unit length, the only possibility for the integration to terminate prematurely is when the flow $\mathbf{x}(t)$ hits a point $\mathbf{x}^*$ where the singular values of $f'(\mathbf{x}^*)$ coalesce. The coalescence causes complicated but interesting phenomena which will be the focal point of discussion in the later part of this paper.

A quick glance at these drawings manifests distinctive and fascinating structures typifying a specific, and perhaps previously unknown, landmark for the corresponding function. We are interested in understanding the cause of these structures.

Toward this goal, write the $n \times 2$ Jacobian matrix of $f(\mathbf{x})$ in its two columns

$$f'(\mathbf{x}) = \left[\ \mathbf{a}_1(\mathbf{x}),\, \mathbf{a}_2(\mathbf{x})\ \right].$$

Define the two scalar functions

$$\begin{cases} n(\mathbf{x}) &:= \|\mathbf{a}_2(\mathbf{x})\|^2 - \|\mathbf{a}_1(\mathbf{x})\|^2 \\ o(\mathbf{x}) &:= 2\mathbf{a}_1(\mathbf{x})^\top \mathbf{a}_2(\mathbf{x}) \end{cases} \tag{2.1}$$

which measure, respectively, the disparity of norms and nearness of orthogonality between the column vectors of $f'(\mathbf{x})$. Generically, each of the two sets defined by

$$\begin{cases} \mathcal{N} &:= \{\mathbf{x} \in \mathbb{R}^n \,|\, n(\mathbf{x}) = 0\} \\ \mathcal{O} &:= \{\mathbf{x} \in \mathbb{R}^n \,|\, o(\mathbf{x}) = 0\} \end{cases} \tag{2.2}$$

forms a 1-dimensional manifold in $\mathbb{R}^2$, possibly composed of, if not empty, multiple curves or loops. They will be shown in our analysis to play the role of "polynucleotide" connecting a string of interesting points and characterizing certain, if not all, properties of a function.

A direct computation shows that the two singular values of $f'(\mathbf{x})$ are given by

$$\begin{cases} \sigma_1(\mathbf{x}) &:= \left(\frac{1}{2}\left(\|\mathbf{a}_1(\mathbf{x})\|^2 + \|\mathbf{a}_2(\mathbf{x})\|^2 + \sqrt{o(\mathbf{x})^2 + n(\mathbf{x})^2}\right)\right)^{1/2}, \\ \sigma_2(\mathbf{x}) &:= \left(\frac{1}{2}\left(\|\mathbf{a}_1(\mathbf{x})\|^2 + \|\mathbf{a}_2(\mathbf{x})\|^2 - \sqrt{o(\mathbf{x})^2 + n(\mathbf{x})^2}\right)\right)^{1/2}. \end{cases} \tag{2.3}$$

Example 1	**Example 2a**	**Example 2b**
$\begin{bmatrix} \sin(x_1+x_2)+\cos(x_2)-1 \\ \cos(2x_1)+\sin(x_2)-1 \end{bmatrix}$	$\begin{bmatrix} e^{x_1}\cos(x_2) \\ 20e^{x_1}\sin(x_1) \end{bmatrix}$	$\begin{bmatrix} e^{x_1}\cos(x_2) \\ e^{x_1}\sin(x_1) \\ x_2 \end{bmatrix}$
Example 3	**Example 4**	**Example 5**
$\begin{bmatrix} 4+x_1\cos(x_2/2) \\ x_2 \\ x_1\sin(x_1x_2/2) \end{bmatrix}$	$\begin{bmatrix} e^{x_1}\cos(20x_2) \\ 20e^{sin(x_2)}\sin(x_1) \end{bmatrix}$	$\begin{bmatrix} \sin(x_1^2+x_2^2)\cos(x_2) \\ 2e^{-2x_2^2x_1^2}\cos(10\sin(x_1)) \end{bmatrix}$
Example 6 [15]	**Example 7**	**Example 8 [11]**
$\begin{bmatrix} \begin{pmatrix} -270x_1^4x_2^3-314x_1x_2^4 \\ -689x_1x_2^3+1428 \end{pmatrix} \\ \begin{pmatrix} 36x_1^7+417x_1^6x_2 \\ -422x_1^5x_2^2-270x_1^4x_2^3 \\ +1428x_1^3x_2^4-1475x_1^2x_2^5 \\ +510x_1x_2^6-200x_1^6 \\ -174x_1^5x_2-966x_1^4x_2^2 \\ +529x_1^3x_2^3+269x_1^2x_2^4 \\ +49x_1x_2^5-267x_2^6 \\ +529x_1^4x_2+1303x_1^2x_2^3 \\ -314x_1x_2^4+262x_2^5 \\ +36x_1^4-788x_1^2x_2^2 \\ -689x_1x_2^3+177x_2^4 \end{pmatrix} \end{bmatrix}$	$\begin{bmatrix} x_1-\frac{x_1^2}{3}+x_1x_2^2 \\ x_2-\frac{x_2^3}{6}+x_2x_1^3 \\ x_1^2-x_2^3 \end{bmatrix}$	$\begin{bmatrix} \begin{pmatrix} \frac{1}{2}(2\rho^2-\phi^2-\psi^2 \\ +2\phi\psi(\phi^2-\psi^2) \\ +\psi\rho(\rho^2-\psi^2) \\ +\rho\phi(\phi^2-\rho^2)) \end{pmatrix} \\ \begin{pmatrix} \frac{\sqrt{3}}{2}(\phi^2-\psi^2 \\ +(\psi\rho(\psi^2-\rho^2) \\ +\rho\phi(\phi^2-\rho^2))) \end{pmatrix} \\ \begin{pmatrix} (\rho+\phi+\psi) \\ *((\rho+\phi+\psi)^3 \\ +4(\phi-\rho)(\psi-\phi) \\ *(\rho-\psi)) \end{pmatrix} \end{bmatrix}$ with $\begin{cases} \rho=\cos(x_1)\sin(x_2) \\ \phi=\sin(x_1)\sin(x_2) \\ \psi=\cos(x_2) \end{cases}$

TABLE 2.1
List of sample functions.

The corresponding right singular vectors are

$$\mathbf{u}_1(\mathbf{x}) \coloneqq \frac{\pm 1}{\sqrt{1+\omega(\mathbf{x})^2}} \begin{bmatrix} \omega(\mathbf{x}) \\ 1 \end{bmatrix}, \tag{2.4}$$

$$\mathbf{u}_2(\mathbf{x}) \coloneqq \frac{\pm 1}{\sqrt{1+\zeta(\mathbf{x})^2}} \begin{bmatrix} \zeta(\mathbf{x}) \\ 1 \end{bmatrix}, \tag{2.5}$$

where, for the convenience of quickly reading off the directions, we normalize the second entry of

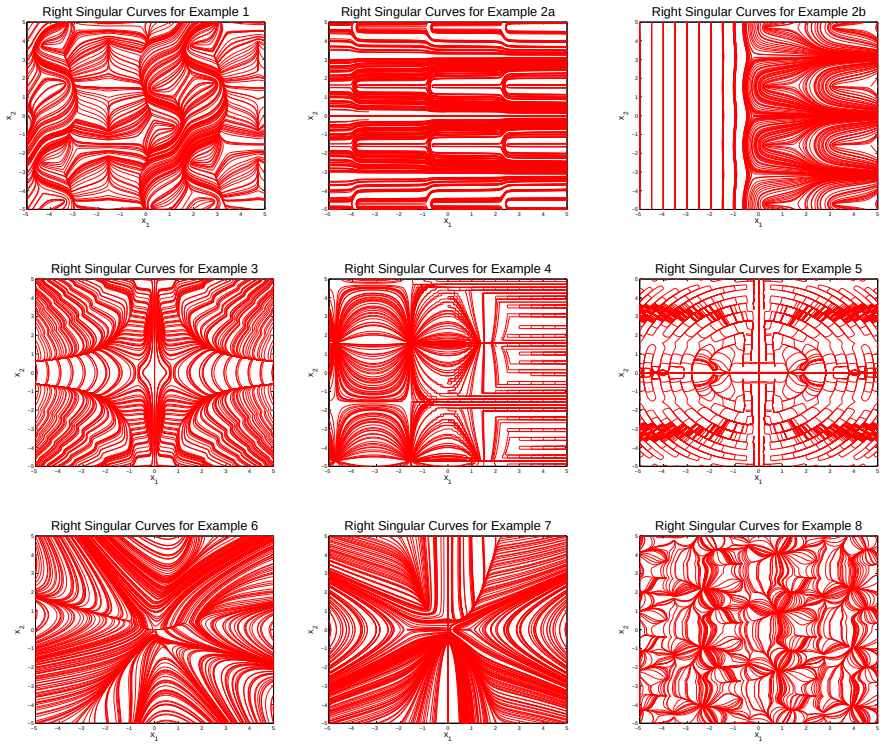


FIG. 2.1. *Examples of right singular curves* $\mathbf{x}_1(t)$.

the singular vectors with the understanding of taking limits if either $\omega(\mathbf{x})$ or $\zeta(\mathbf{x})$ defined by

$$\begin{cases} \omega(\mathbf{x}) & := \begin{cases} \frac{o(\mathbf{x})}{n(\mathbf{x})+\sqrt{o(\mathbf{x})^2+n(\mathbf{x})^2}}, & \text{if } n(\mathbf{x}) > 0, \\ \frac{-n(\mathbf{x})+\sqrt{o(\mathbf{x})^2+n(\mathbf{x})^2}}{o(\mathbf{x})}, & \text{if } n(\mathbf{x}) < 0, \end{cases} \\ \zeta(\mathbf{x}) & := \begin{cases} \frac{-n(\mathbf{x})-\sqrt{o(\mathbf{x})^2+n(\mathbf{x})^2}}{o(\mathbf{x})}, & \text{if } n(\mathbf{x}) > 0, \\ \frac{o(\mathbf{x})}{n(\mathbf{x})-\sqrt{o(\mathbf{x})^2+n(\mathbf{x})^2}}, & \text{if } n(\mathbf{x}) < 0 \end{cases} \end{cases} \tag{2.6}$$

becomes infinity. Expressions for both $\mathbf{u}_1$ and $\mathbf{u}_2$ are given, but we will carry out the analysis for $\mathbf{x}_1(t)$ only as that for $\mathbf{x}_2(t)$ can be done similarly.

It follows immediately from (2.4) that the tangent vectors to the singular curves at any points in $\mathcal{N}$ but not in $\mathcal{O}$ are always parallel to either $[1, 1]^\top$ or $[1, -1]^\top$, depending on whether $o(\mathbf{x})$ is positive or negative. Likewise, the tangent vectors of the singular curves at any points in $\mathcal{O}$ but not in $\mathcal{N}$ are parallel to $[0, 1]^\top$ or $[1, 0]^\top$, depending on whether $n(\mathbf{x})$ is positive or negative. At places where $\mathcal{N}$ and $\mathcal{O}$ intersect, which will be called *singular points*, the singular values coalesce and the (right) singular vectors become ambiguous. In the following we argue that it is the angles cut by $\mathcal{N}$ and $\mathcal{O}$ at the singular point that affect the intriguing dynamics observed in Figure 2.1. The 1-dimensional manifolds $\mathcal{N}$ and $\mathcal{O}$ can be thought of as stringing singular points together (with particular pairings) and will be referred to as the *critical curves* of f.

Corresponding to the functions in Table 2.1, we plot the critical curves in Figure 2.2. Also drawn, but sometimes not so conspicuous due to tininess, are the borders surrounding the sin-

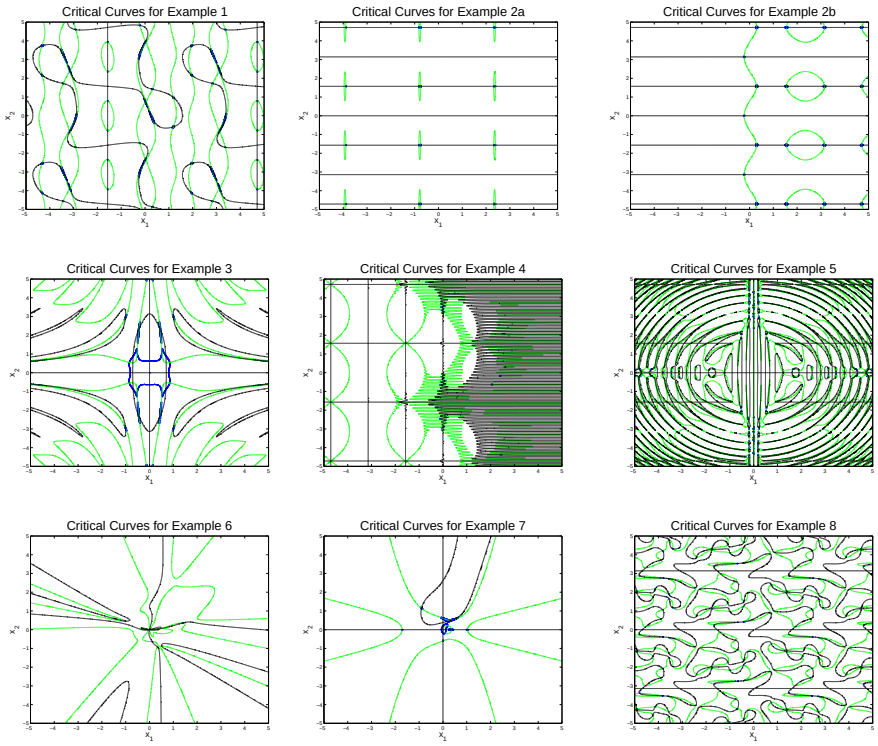


FIG. 2.2. *Examples of critical curves:* $n(\mathbf{x}) = 0$ *(green);* $o(\mathbf{x}) = 0$*, (black); borders where* $\sigma_2/\sigma_1 \geq .95$*, (blue, not always shown if the region is too small).*

gular points within which the ratio $\sigma_2/\sigma_1 > 0.95$ is high. These regions are where the numerical calculation of singular vectors become less trustworthy.

By overlaying the drawings in Figures 2.1 with those in Figure 2.2, we can catch a glimpse into the effect of these critical curves on the dynamics. To demonstrate our point, we reconsider Example 1 over a coarser grid of initial values in Figure 2.3. Take notice of the angles when the singular curves cut across the critical curves. Note also that there are portions where the critical curves are extremely close to each other, forming long and narrow ridges with $\sigma_2/\sigma_1 > 0.95$.

3. Local Behavior. Let $\mathbf{x}_0$ be an isolated singular point. We now investigate the dynamical behavior nearby $\mathbf{x}_0$. Consider the scenario where $\mathcal{N}$ and $\mathcal{O}$ intersect in the scheme sketched in Figure 3.1. The short red segments denote tangent vectors of singular curves crossing the critical curves after taking into account the signs of $o(\mathbf{x})$ and $n(\mathbf{x})$. These directions are invariant on each halves of the critical curves. The portions of $\mathcal{N}$ and $\mathcal{O}$ where the tangent vectors of the crossing singular curves are parallel to the unit vectors $\mathbf{u}_{n_\alpha} := \frac{1}{\sqrt{2}}[1,1]^\top$ and $\mathbf{u}_{o_\alpha} := [0,1]^\top$, respectively, are referred to as the *α-halves* of the critical curves and denoted by n_α and o_α. Likewise, by changing α to β, we refer to the other halves of the critical curves. It is convenient to flag the critical curves by arrows to indicate the sides of n_α and o_α. The neighborhood of $\mathbf{x}_0$ is naturally divided into "quadrants" distinguished by the signs $(\mathrm{sgn}(n(\mathbf{x})), \mathrm{sgn}(o(\mathbf{x}))$ which, in a sense, imply a specific "orientation" of a local curvilinear coordinate system. With tangent vectors depicted in Figure 3.1, the flow of the singular curves near $\mathbf{x}_0$ should move away from $\mathbf{x}_0$ as is depicted in the right diagram. In other words, the singular point $\mathbf{x}_0$ acts like a repeller for the flows $\mathbf{x}_1(t)$. When the orientation is changed, the nearby dynamical behavior might change its topology such as that

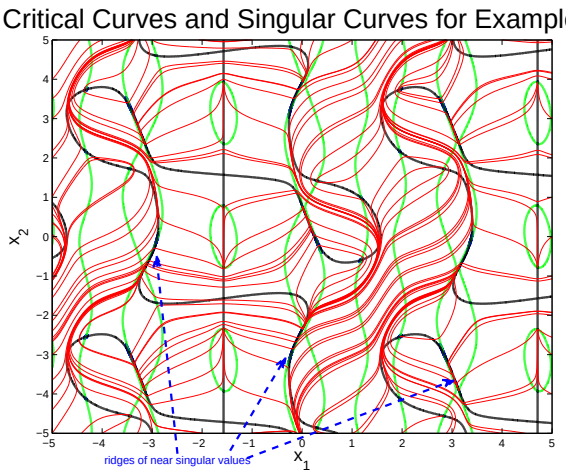


FIG. 2.3. *Superposition of singular curves and critical curves for example 1:* $n(\mathbf{x}) = 0$ *(green);* $o(\mathbf{x}) = 0$*, (black); singular curves (red); ridges of near singular values (pointed by blue arrows).*

depicted in Figure 3.2. The general scenarios are summarized in Figure 3.3.

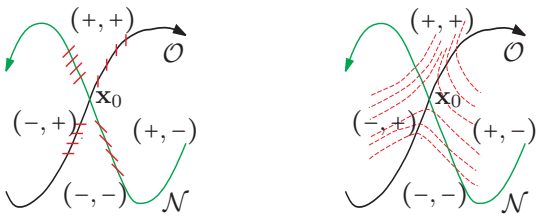


FIG. 3.1. *Local behavior nearby a propellent singular point* $\mathbf{x}_0$.

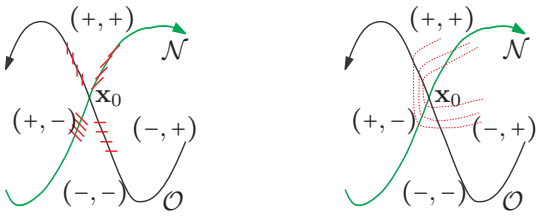


FIG. 3.2. *Local behavior nearby a roundabout singular point* $\mathbf{x}_0$.

In an infinitesimal sense, manifolds $\mathcal{N}$ and $\mathcal{O}$ near $\mathbf{x}_0$ can be represented by their respective tangent vectors $\boldsymbol{\tau}_n$ and $\boldsymbol{\tau}_o$ at $\mathbf{x}_0$. Again we flag the originally undirected vectors $\boldsymbol{\tau}_n$ and $\boldsymbol{\tau}_o$ with arrows pointing to the corresponding α-halves of the critical curves. Starting with the north and centered at $\mathbf{x}_0$, divide the plane into eight sectors, each with a central angle $\frac{\pi}{4}$, and assign an ordinal number to name the sectors clockwise. The relative position of the two α-halves n_α and o_α with respect to these sectors is critical for deciding the local behavior.

Consider first the generic case when $\boldsymbol{\tau}_n$ is not parallel to $\mathbf{u}_{n_\alpha}$ and $\boldsymbol{\tau}_o$ is not parallel to $\mathbf{u}_{o_\alpha}$. Special cases will be amended in the sequel. Because qualitative behaviors of singular curves within

fixed sectors are similar, it suffices to examine a total of 80 possible configurations identified by the label (i, j) when $\boldsymbol{\tau}_n$ and $\boldsymbol{\tau}_o$ are located in the i-th and the j-th sectors, respectively. As already demonstrated earlier in Figures 3.1 and 3.2, orientations of $\boldsymbol{\tau}_n$ and $\boldsymbol{\tau}_o$ do matter. For clarity, we divide the configurations into three sections. There are 48 off-diagonal sketches at the top section of Figure 3.3 for the cases $i \neq j$ and $|i-j| \neq 4$, including $\boldsymbol{\tau}_n$ and $\boldsymbol{\tau}_o$ in reverse positions. Separated respectively in the middle and bottom sections of Figure 3.3 are the 16 sketches in addition to the cases $i = j$ and $|i-j| = 4$ with the positions of $\boldsymbol{\tau}_n$ and $\boldsymbol{\tau}_o$ swapped. The local bearings are identified by the two-letter mark at the upper left corner in each configuration, which will be explained next.

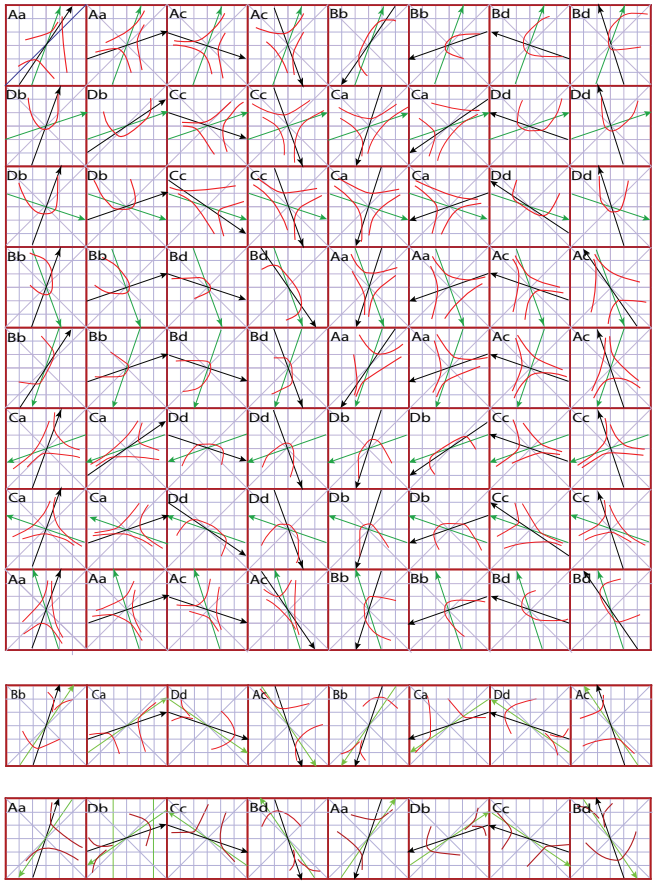


FIG. 3.3. *80 possible local behaviors nearby a singular point* $\mathbf{x}_0$. *Arrows point at the* α*-halves of* $n(\mathbf{x}) = 0$ *(green) and* $o(\mathbf{x}) = 0$ *(black).*

4. Base Pairing. Observe that $\omega(\mathbf{x})$ can be expressed as

$$\omega(\mathbf{x}) := \begin{cases} \operatorname{sgn}\big(o(\mathbf{x})\big) - \frac{n(\mathbf{x})}{o(\mathbf{x})} + \frac{\operatorname{sgn}(o(\mathbf{x}))n(\mathbf{x})^2}{2o(\mathbf{x})^2} + O\Big(n(\mathbf{x})^3\Big), & \text{near } n(\mathbf{x}) = 0, \\ \frac{o(\mathbf{x})}{2n(\mathbf{x})} - \frac{o(\mathbf{x})^3}{8n(\mathbf{x})^3} + \frac{o(\mathbf{x})^5}{16n(\mathbf{x})^5} + O\Big(o(\mathbf{x})^7\Big), & \text{near } o(\mathbf{x}) = 0 \text{ and if } n(\mathbf{x}) > 0, \\ \frac{-1}{\frac{o(\mathbf{x})}{2n(\mathbf{x})} - \frac{o(\mathbf{x})^3}{8n(\mathbf{x})^3} + \frac{o(\mathbf{x})^5}{16n(\mathbf{x})^5} + O\big(o(\mathbf{x})^7\big)}, & \text{near } o(\mathbf{x}) = 0 \text{ and if } n(\mathbf{x}) < 0. \end{cases} \tag{4.1}$$

We already know that the first derivative of $\mathbf{x}_1(t)$ is related to $\omega(\mathbf{x}_1(t))$ via (2.4). The expansion (4.1) of $\omega(\mathbf{x})$ can now be used to estimate the second derivative of $\mathbf{x}_1(t)$. In this way, we can characterize the concavity property and the local behaviors observed in Figure 3.3.

As an example, starting from a point on n_α where the singular flow points in the direction $\mathbf{u}_{n_\alpha}$, then $\omega(\mathbf{x}(t))$ increases as $\mathbf{x}(t)$ moves to the side where $n(\mathbf{x}) < 0$, implying that the slope of $\mathbf{u}_1(\mathbf{x}(t))$ must be less than 1. It is instructive to summarize the mutual responses between $\omega(\mathbf{x})$ and the slopes of $\mathbf{u}_1(\mathbf{x})$ near $\mathcal{N}$ in Figure 4.1. In all, near a singular point $\mathbf{x}_0$ and relative to a fixed $\boldsymbol{\tau}_n$, there are only four basic ways, marked as A, B, C, and D, that the singular curves can cross the critical curve $\mathcal{N}$. Noting that $\boldsymbol{\tau}_n$ can be rotated to point in other directions, we sketch a few possible concavities of $\mathbf{x}_1(t)$ in Figure 4.2.

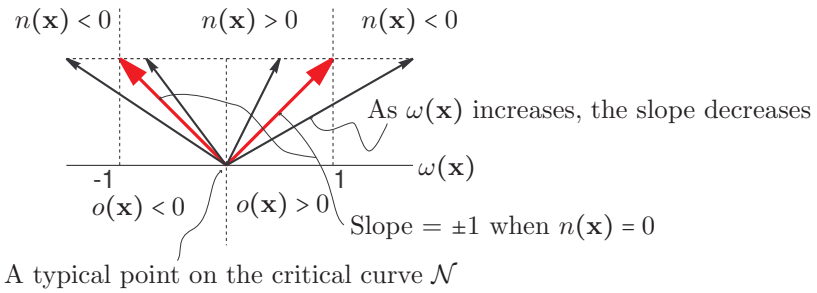


FIG. 4.1. *Variations of $\omega(\mathbf{x})$ and associated slopes of $\mathbf{u}_1(\mathbf{x})$ near the critical curve $n(\mathbf{x}) = 0$.*

Similarly, the values of $\omega(\mathbf{x})$ and the associated slopes of $\mathbf{u}_1(\mathbf{x})$ near $\mathcal{O}$ must vary in the way indicated in Figures 4.3. Again, there are four basic concavities of $\mathbf{x}_1(t)$ marked as a, b, c, and d, near $\mathcal{O}$, subject to rotations, as depicted in Figure 4.4.

It is the combined effect of these basic curvatures, which we refer to as *base pairing*, together with the positions of $\boldsymbol{\tau}_n$ and $\boldsymbol{\tau}_o$, that makes up the dynamics observed in Figure 3.3. Indeed, the following result is but by a thoroughgoing examination of the 80 dynamics in Figure 3.3.

THEOREM 4.1. *Assume that $\boldsymbol{\tau}_n$ is not parallel to $\mathbf{u}_{n_\alpha}$ and $\boldsymbol{\tau}_o$ is not parallel to $\mathbf{u}_{o_\alpha}$. Then the local behavior of the singular curves can be classified into 8 categories. These base parings are Aa, Ac, Bb, Bd, Ca, Cc, Db, and Dd only, with no other possible combinations.*

Each drawing in Figure 3.3 is identified by two letters of base paring at the upper left corner to indicate the corresponding dynamics. Indeed, a quick count shows that each base pairing results in 8 dynamics in the top drawing as general cases and 2 in the middle or bottom drawings as special cases, distinctive by their characteristic traits.

5. Generality and Idiosyncrasy. We now explain how base pairings affect the classification of dynamics categorized in Figure 3.3. We claim that a single quantity — the angle $\theta(n_\alpha, o_\alpha)$ measured clockwise from $\boldsymbol{\tau}_n$ to $\boldsymbol{\tau}_o$ — characterizes the general behavior, but there are idiosyncrasies that need to be detailed.

THEOREM 5.1. *Assuming the generic condition that $\boldsymbol{\tau}_n$ is not forming an angle of $\frac{\pi}{4}$ with the north, we claim that $\mathbf{x}_0$ is a repeller, if $0 < \theta(n_\alpha, o_\alpha) < \pi$; and a roundabout, if $\theta(n_\alpha, o_\alpha) > \pi$.*

As the proof is readily generalizable to all other cases, it suffices to examine the pairing Aa only. The basic tool employed is the continuity argument. To facilitate the discussion, we define that a signed plane angular measurement is *east-oriented* if angles are positive when measured counter-clockwise with respect to the positive x axis; and negative, otherwise. A *west-oriented* angular measurement is defined similarly, but uses the negative x axis as the reference direction.

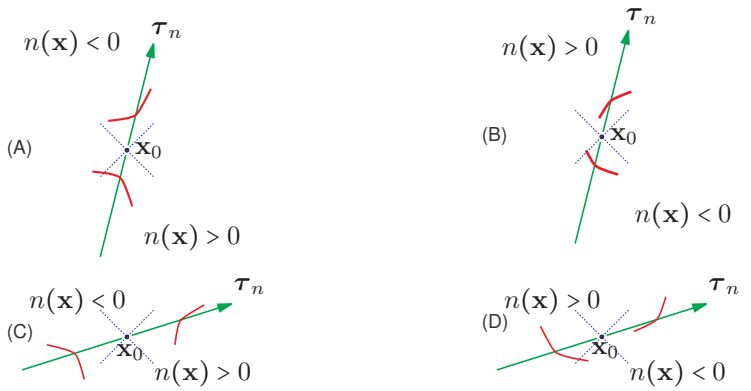


FIG. 4.2. *Basic concavities of singular curves near* $n(\mathbf{x}) = 0$.

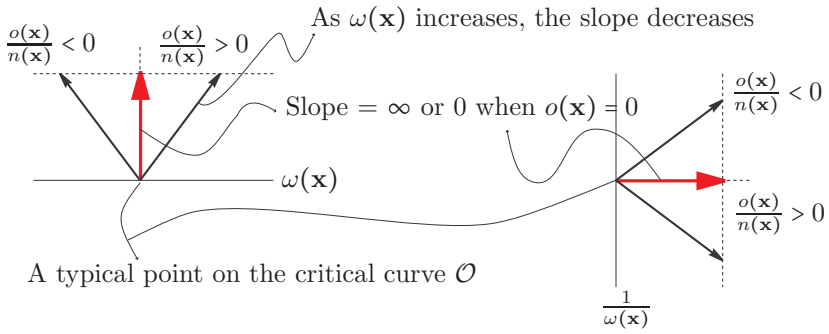


FIG. 4.3. *Variations of* $\omega(\mathbf{x})$ *and associated slopes of* $\mathbf{u}_1(\mathbf{x})$ *near the critical curve* $o(\mathbf{x}) = 0$.

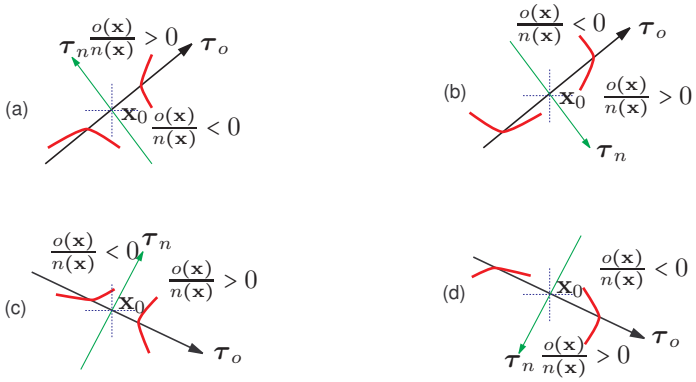


FIG. 4.4. *Basic concavities of singular curves near* $n(\mathbf{x}) = 0$.

The pairing Aa satisfies the criterium $0 < \theta(n_\alpha, o_\alpha) < \pi$. So we claim that the singular point $\mathbf{x}_0$ is a repeller. We consider the general case and the special case separately.

For the general case of Aa pairing, let $\boldsymbol{\gamma}(s)$, $s \in [0,1]$, be an arbitrary segment connecting the critical curves n_α and o_α with $\boldsymbol{\gamma}(0) \in n_\alpha$ and $\boldsymbol{\gamma}(1) \in o_\alpha$. Let $\theta_{\boldsymbol{\gamma}}(s)$ represent the direction angle of the array $\boldsymbol{\gamma}(s) - \mathbf{x}_0$ and $\theta_{\mathbf{u}}(s)$ the tangent angle of the singular vector $\mathbf{u}_1(\boldsymbol{\gamma}(s))$, all measured with

east-orientation if $\boldsymbol{\tau}_n$ resides in Sectors 1 or 8; and with west-orientation if $\boldsymbol{\tau}_n$ resides in Sectors 4 or 5. So $\theta_{\boldsymbol{\gamma}} \in (-\frac{3\pi}{4}, \frac{3\pi}{4})$ and $\theta_{\mathbf{u}} \in [\frac{\pi}{4}, \frac{\pi}{2}]$. The function defined by

$$\rho_{\boldsymbol{\gamma}}(s) = \theta_{\boldsymbol{\gamma}}(s) - \theta_{\mathbf{u}}(s), \quad s \in [0,1] \tag{5.1}$$

is continuous and has the properties $\rho_{\boldsymbol{\gamma}}(0) > 0$ and $\rho_{\boldsymbol{\gamma}}(1) < 0$ at the endpoints of the interval $[0,1]$. Therefore, there exists an intermediate value $\widehat{s} \in (0,1)$ such that $\rho_{\boldsymbol{\gamma}}(\widehat{s}) = 0$, that is, $\boldsymbol{\gamma}(\widehat{s}) - \mathbf{x}_0$ is parallel to $\mathbf{u}_1(\boldsymbol{\gamma}(\widehat{\boldsymbol{s}}))$. Continuously deforming the segment $\boldsymbol{\gamma}(s)$ in a parallel manner toward the singular point $\mathbf{x}_0$, we conclude that there is a curve $\boldsymbol{\phi}(\epsilon)$ of the form

$$\boldsymbol{\phi}(\epsilon) = \mathbf{x}_0 + c(\epsilon)\mathbf{u}_1(\boldsymbol{\phi}(\epsilon)) \tag{5.2}$$

residing in the quadrant between n_α and o_α with a scalar function $c(\epsilon)$ converging to zero as $\epsilon \to 0$. This particular curve satisfying (5.2) is referred to as a *bifurcation curve* at $\mathbf{x}_0$, because the singular flows have different local behaviors on its two sides. Totally there are three bifurcation curves at $\mathbf{x}_0$.

Take the case that $\boldsymbol{\tau}_n$ is in Sector 1 to demonstrate the idea. Observe that this bifurcation curve cannot have any point in Sector 2. The reason is that if the segment and the northeast line ever intersect, say, at $\boldsymbol{\gamma}(\widetilde{s})$, then we must have $\theta_{\boldsymbol{\gamma}}(\widetilde{s}) = \frac{\pi}{4}$ and $\rho_{\boldsymbol{\gamma}}(\widetilde{s}) = \frac{\pi}{4} - \theta_{\mathbf{u}}(\widetilde{s}) \le 0$, implying that $\widehat{s} \in (0, \widetilde{s}]$. This observation explains why the arrowheads of Aa in both $(1,1)$ and $(1,2)$ diagrams of Figure 3.3 slant more toward the north-northeast direction.

For the special cases of Aa pairing, there are two bifurcation curves between n_α and o_α. One can readily be justified by the sign change of the function $\rho_{\boldsymbol{\gamma}}(s)$ defined in (5.1). The second bifurcation curve can be seen by noting that the modified function

$$\varrho_{\boldsymbol{\gamma}}(s) = \theta_{\boldsymbol{\gamma}}(s) - \theta_{\mathbf{u}}(s) + \pi \tag{5.3}$$

also changes its signs over the interval $[0,1]$, implying the existence of a point $\overline{s} \in (0,1)$ different from the root $\widehat{s}$ of $\rho_{\boldsymbol{\gamma}}(s)$ such that $\boldsymbol{\gamma}(\overline{s}) - \mathbf{x}_0$ is parallel to $\mathbf{u}_1(\boldsymbol{\gamma}(\overline{\boldsymbol{s}}))$.

In all, the basic principle is to check appropriate angles with respect to appropriate reference axes to show the existence of a bifurcation curve in between corresponding half curves. The argument can be used repetitively to verify all diagrams in Figure 3.3.

The criterium $0 < \theta(n_\alpha, o_\alpha) < \pi$ includes 40 cases all of which share the structure of having three bifurcations curves near $\mathbf{x}_0$ dividing the neighborhood into three regions. In each region the singular curves is pushed away from $\mathbf{x}_0$ which thus is called a repeller.

The remaining 40 cases for the criterium $\theta(n_\alpha, o_\alpha) > \pi$ involve somewhat more complicated dynamics. We refer to $\mathbf{x}_0$ as a roundabout because that there is always one singular curve making a U-turn around $\mathbf{x}_0$. It is possible that there are additional dynamical properties nearby, including one or more bifurcation curves or even an asymptotic contraction. All can be checked by the same idea of proof and we skip the details.

Taking another closer look at the Aa base pairing again, we find that the singular curves nearby the repeller form an "arrowhead". The general trait is that the tip points to in-between quadrant of n_α and o_α while the base sitting across both n_β and o_β halves simultaneously. The special trait, distinguished by Aa/s if necessary, is that the tip points to in-between quadrant of n_β and o_β while its base resides in the $(+,+)$ quadrant with its edges crossing either n_β or o_β.

In contrast, if we examine the Bb base pairing, then the general trait for the roundabout is that the turning point resides in between n_α and o_α. The special trait for Bb/s, on the other hand, is that the singular point $\mathbf{x}_0$ is a hybrid of an attractor from in between n_α and o_α, and a roundabout from in between n_β and o_β.

Sometimes the traits between two distinct pairings look alike, but there are subtle differences. The base of the arrowhead for the general Ac pairing, for example, differs from that of the Aa pairing in that it crosses the β-half n_β only.

For the non-generic cases not covered in Figure 3.3, the sign of $\rho_{\boldsymbol{\gamma}}(0)$ cannot be ascertained by the information of $\boldsymbol{\tau}_n$ and $\boldsymbol{\tau}_o$ alone. Rather, more precise knowledge of the relative position between the critical curves and their tangents is needed. As a demonstration, consider the situation when $\boldsymbol{\tau}_n$ points to the north-east whereas $\boldsymbol{\tau}_o$ is not aligned with the east, the west, or the $\boldsymbol{\tau}_n$ direction. There are eight possible schemes. See Figure 5.1. Local behaviors of singular curves depend not only on the relative position of $\boldsymbol{\tau}_0$ to $\boldsymbol{\tau}_n$ but also on which side of $\boldsymbol{\tau}_n$ that the α-half n_α resides.

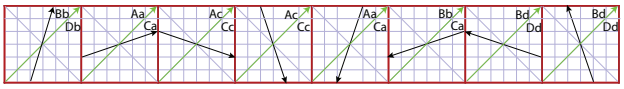


FIG. 5.1. *Relative positions of $\boldsymbol{\tau}_o$ and possible transitions of base pairings when $\boldsymbol{\tau}_n$ points to the north-east.*

We select two cases to show the subtlety. In the rightmost configuration of Figure 5.1, if n_α resides on the left side of $\boldsymbol{\tau}_n$, then we have the Bd dynamics similar to that of $(1, 8)$ in Figure 3.3; but if n_α veers to the right of $\boldsymbol{\tau}_n$, then we have the Dd dynamics similar to that of $(2, 8)$ in Figure 3.3. We denote this as a hybrid Bd/Dd base pairing. The topology of $\mathbf{x}_0$ being a roundabout is invariant, but the traits are changed. Similarly, in the fifth configuration from the left, we have $\mathbf{x}_0$ as a repeller changing from Aa to Ca. We summarize this "crossover" of pairings on the two sides of $\boldsymbol{\tau}_n$ in Figure 5.1.

For completion, the hybrid base parings when $\boldsymbol{\tau}_o$ points in the north-south direction are also summarized in Figure 5.2. Without furnishing further mundane details, we remark that even for the extreme situations such as when $\boldsymbol{\tau}_n$ and $\boldsymbol{\tau}_o$ are parallel to each other, the dynamics can be explained by the idea outlined above.

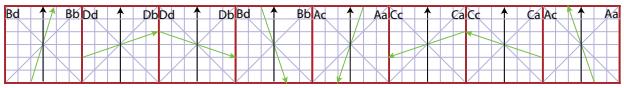


FIG. 5.2. *Relative positions of $\boldsymbol{\tau}_n$ and possible transitions of base pairings when $\boldsymbol{\tau}_o$ points to the north.*

6. Applications. The classification of all possible local behaviors suggests a simplistic collection of "tiles" for the delicate and complex "mosaics" observed in Figure 2.2. In reality, it is the inherent characteristics of the underlying function that arrange these local pieces together along the strands of $\mathcal{N}$ and $\mathcal{O}$ to form the various patterns. Far from complete understanding, we apply the above analysis to examine a few more details.

The dynamics of singular curves for elementary surfaces, such as those quadric surfaces taught in calculus, are fairly easy to analyze. Readers are encouraged to conduct experiments for themselves. We have put a software package including numerical integrator and graphic tools developed for general surfaces on the web site [2] for interested readers to download.

For more complicated problems, examples 2a and 2b serve as a good contrast between the dynamics, despite of their similarity. Their critical curves are the easiest to describe in words. In both examples, the set $\mathcal{O}$ forms horizontal lines whereas $o(\mathbf{x})$ alternates signs over the spaces in between, starting with the negative in the horizontal strip immediately above the line $x_2 = 0$. Meanwhile, the set $\mathcal{N}$ forms closed loops as well as one additional vertical, continuous, ogee curve in Example 2b. It can be checked that $n(\mathbf{x}) > 0$ inside the loops and to the left of the ogee curve. Taking advantage of the obvious periodicity, we could zoom in for a close-up over smaller windows. A few sample curves are plotted in Figure 6.1.

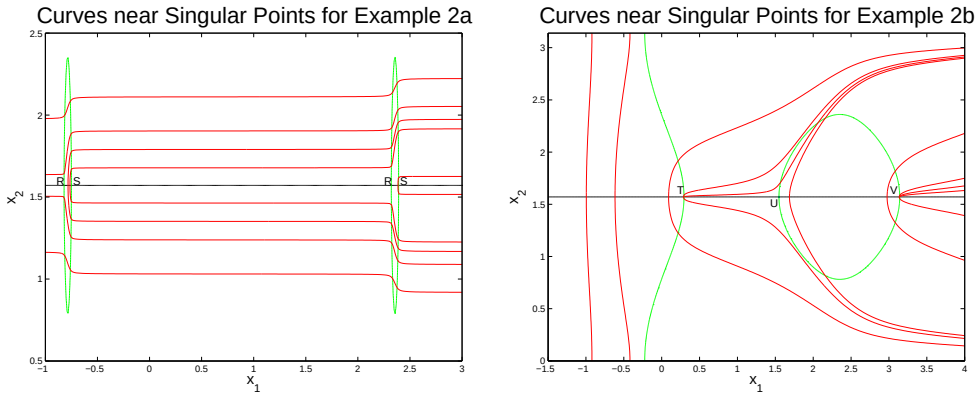


FIG. 6.1. *Samples of singular curves (red) and singular points in Example 2a (left) and Example 2b (right):* $n(\mathbf{x}) = 0$ *(green);* $o(\mathbf{x}) = 0$*, (black).*

Singular points R and S in Example 2a are of the hybrid Aa/Ac and Bb/Bd base pairings, respectively. Note that a singular curve nearby R gets repelled to the left until it reaches close enough to S, whence makes a U-turn back to R to be further repelled to the right. Singular points T, U, and V in Example 2b are of Bb/Bd, Aa/Ac, and Bb/Bd base pairings, respectively. Despite of their seemingly different appearances, all S, T, and V are topologically equivalent roundabouts.

Observe, however, that there are regions nearby R and U, both having the same type of base pairing, from which singular curves are attracted leftward to S and T, respectively, and do *not* make U-turns. The existence of such a basin of contraction needs further understanding.

Critical curves $\mathcal{N}$ and $\mathcal{O}$ generally intertwine in a much more involved way. Determining their α-halves is a much more difficult task. This is precisely where the inherent nature of the underlying function defines the beauty and complexity of its mosaic patterns. We illustrate our point by color coding the the jigsaw pieces over the window $[-2, 4] \times [-2, 4]$ in Figure 6.2 to evince the signs of $n(\mathbf{x})$ and $o(\mathbf{x})$. Singular points occurs at the common borders where the regions overlap, whose orientations are thus determined. We look up from Figure 3.3 to label the singular points with corresponding base pairings, thus having full knowledge of which pieces are in the puzzle.

Though we have all the local pieces in hand, we hasten to point out that something is still missing. As can be seen in Figure 6.2, the two Bd local solutions near the point $(0, 1)$ wander off to distinct destinations with contractions. This long term dynamics must have other astounding bearings not explainable by our current analysis yet.

7. Concluding remark. Gradient adaption is an important mechanism occurring frequently in nature, arts, and sciences. Its generalization to Jacobian for vector functions does not rank the critical directions immediately. That information is encoded in the moving frame of singular vectors. Intricate patterns resulting from singular curves seem to characterize some underneath movement of the function.

Though the global behavior in general and its interpretation in specific are yet to be further understood, we explain that, for parameterized surfaces in $\mathbb{R}^3$ at least and for any $f : \mathbb{R}^2 \to \mathbb{R}^n$ in general, two strands joined by singular points with one of eight distinct base pairings make up the behavior of the function. This is amazingly analogous to the DNA structure essential for all known forms of life.

Are the patterns discovered the trace of DNA within a given function? It would be interesting, and certainly appealing, to apply such a concept of "genome sequencing" to characterize abstract functions.

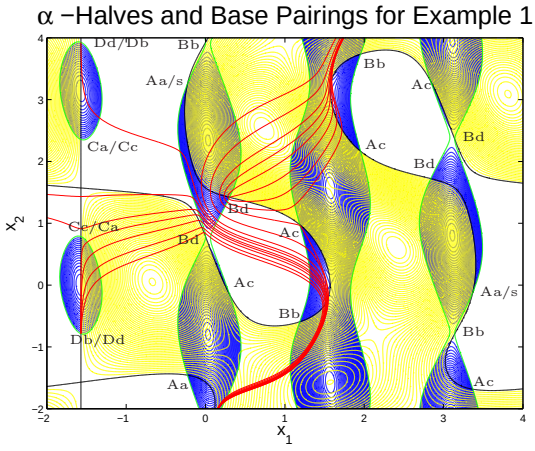


FIG. 6.2. *Base pairings for sample singular points in Example 1:* $n(\mathbf{x}) = 0$ *(green);* $n(\mathbf{x}) > 0$ *(blue);* $o(\mathbf{x}) = 0$*, (black);* $o(\mathbf{x}) > 0$*, (yellow).*

REFERENCES

[1] A. BUNSE-GERSTNER, R. BYERS, V. MEHRMANN, AND N. K. NICHOLS, *Numerical computation of an analytic singular value decomposition of a matrix valued function*, Numer. Math., 60 (1991), pp. 1–39.

[2] M. T. CHU, *Shape dna integrators and graphic tools*, North Carolina State Univesity, available at `http://www4.ncsu.edu/~mtchu/Research/Library/Readme.htm`, 2011.

[3] L. ELDÉN, *Matrix methods in data mining and pattern recognition*, vol. 4 of Fundamentals of Algorithms, Society for Industrial and Applied Mathematics (SIAM), Philadelphia, PA, 2007.

[4] G. H. GOLUB AND C. F. VAN LOAN, *Matrix computations*, Johns Hopkins Studies in the Mathematical Sciences, Johns Hopkins University Press, Baltimore, MD, third ed., 1996.

[5] D. X. GU, W. ZENG, L. M. LUI, F. LUO, AND S.-T. YAU, *Recent development of computational conformal geometry*, in Fifth International Congress of Chinese Mathematicians. Part 1, 2, vol. 2 of AMS/IP Stud. Adv. Math., 51, pt. 1, Amer. Math. Soc., Providence, RI, 2012, pp. 515–560.

[6] X. D. GU AND S.-T. YAU, *Computational conformal geometry*, vol. 3 of Advanced Lectures in Mathematics (ALM), International Press, Somerville, MA, 2008. With 1 CD-ROM (Windows, Macintosh and Linux).

[7] T. HASTIE AND W. STUETZLE, *Principal curves*, J. Amer. Statist. Assoc., 84 (1989), pp. 502–516.

[8] T. J. HASTIE, *Principa Curves and Surfaces*, PhD thesis, Stanford University, available at `http://www.slac.stanford.edu/pubs/slacreports/slac-r-276.html`, 1984.

[9] B. KÉGL, *Principal curves*, Université Paris Sud 11, available at `http://www.iro.umontreal.ca/~kegl/research/pcurves/`, 2012.

[10] V. C. KLEMA AND A. J. LAUB, *The singular value decomposition: its computation and some applications*, IEEE Trans. Automat. Control, 25 (1980), pp. 164–176.

[11] A. J. MACLEAN, *Parametric equations for surfaces*, University of Sydney, available at `http://www.vtk.org/VTK/img/ParametricSurfaces.pdf`, 2006.

[12] M. REUTER, F.-E. WOLTER, AND N. PEINECKE, *Laplace-beltrami spectra as "shape-dna" of surfaces and solids*, Computer-Aided Design, 38 (2006), pp. 342–366. Symposium on Solid and Physical Modeling 2005.

[13] G. W. STEWART, *On the early history of the singular value decomposition*, SIAM Rev., 35 (1993), pp. 551–566.

[14] J. VANDEWALLE AND B. DE MOOR, *On the use of the singular value decomposition in identification and signal processing*, in Numerical linear algebra, digital signal processing and parallel algorithms (Leuven, 1988), vol. 70 of NATO Adv. Sci. Inst. Ser. F Comput. Systems Sci., Springer, Berlin, 1991, pp. 321–360.

[15] J. VERSCHELDE, *The database of polynomial systems*, University of Illinois at Chicago, available at `http://www.math.uic.edu/~jan/demo.html`, 2011.

[16] M. E. WALL, A. RECHTSTEINER, AND L. M. ROCHA, *Singular value decomposition and principal component analysis*, in A Practical Approach to Microarray Data Analysis, D. P. Berrar, W. Dubitzky, and M. Granzow, eds., Kluwer, Norwell, MA, available at `http://www.springerlink.com/content/x035256j0h64h187/` ed., 2003, ch. 5, pp. 91–108.

[17] K. WRIGHT, *Differential equations for the analytic singular value decomposition of a matrix*, Numer. Math., 63 (1992), pp. 283–295.